

Engineered spin-valve type magnetoresistance in $\text{Fe}_3\text{O}_4\text{-CoFe}_2\text{O}_4$ core-shell nanoparticles

P. Anil Kumar,^{1,2} Sugata Ray,^{1,3} S. Chakraverty,^{1,4} and D. D. Sarma^{1,5,6,7, a)}

¹⁾ *Centre for Advanced Materials, Indian Association for the Cultivation of Science, Kolkata, 700032, India*

²⁾ *Department of Engineering Sciences, Uppsala University, P.O. Box 534, SE-751 21 Uppsala, Sweden*

³⁾ *Department of Materials Science, Indian Association for the Cultivation of Science, Kolkata, 700032, India*

⁴⁾ *RIKEN Center for Emergent Matter Science (CEMS), Wako 351-0198, Japan*

⁵⁾ *Solid State and Structural Chemistry Unit, Indian Institute of Science, Bangalore, 560012, India*

⁶⁾ *Department of Physics and Astronomy, Uppsala University, Box - 516, 75120 Uppsala, Sweden*

⁷⁾ *Council for Scientific and Industrial Research - Network of Institutes for Solar Energy (CSIR-NISE), New Delhi, India*

(Dated: 31 August 2018)

Naturally occurring spin-valve-type magnetoresistance (SVMR), recently observed in $\text{Sr}_2\text{FeMoO}_6$ samples, is suggestive of the possibility of decoupling the maximal resistance from the coercivity of the magnetic metallic grains, thereby providing an additional handle to tune the MR of a material for technological advantages. In this paper, we present the first evidence that this can indeed be achieved in specifically designed and fabricated core-shell nanoparticle systems, realized here in terms of Fe_3O_4 - CoFe_2O_4 core-shell nanocrystals. Here, the soft magnetic Fe_3O_4 nanocrystals form the core, with the hard magnetic and highly insulating CoFe_2O_4 as the shell, providing a magnetically switchable tunnel barrier that controls the magnetoresistance of the system, instead of the magnetic properties of the magnetic grain material, Fe_3O_4 , and thus proving the feasibility of engineered SVMR structures.

^{a)}Also at Jawaharlal Nehru Centre for Advanced Scientific Research, Bangalore. Electronic mail: sarma@sscu.iisc.ernet.in

The tunneling magnetoresistance (TMR) phenomenon¹ became technologically attractive after the realization of large magnetoresistance values.² In most of the naturally occurring polycrystalline TMR materials such as Fe_3O_4 , CrO_2 , $\text{La}_{0.67}\text{Sr}_{0.33}\text{MnO}_3$,³⁻⁶ the grain boundaries are found to act as the insulating, non-magnetic barrier. An important characteristic of such TMR systems is that the magnetoresistance, MR , has a peak at the magnetic coercivity (H_C) of the grain material.³⁻⁵ As a consequence, the MR response of the system to an external magnetic field cannot be, in general, varied independent of the coercive field of the ferromagnetic metallic grains. However, it would be desirable to have this flexibility of choosing the zero of the MR independent of the magnetic properties of the grain material, thereby providing us with an additional handle to design applications of such materials. For such manipulations of MR as a function of H we have recently shown⁷ that the concept of “dipolar biasing” can be used very efficiently; however, this approach works well only in the very low magnetic field regime due to the intrinsic low strength of dipolar interactions compared to exchange interactions. An alternate approach suggests itself based on a different type of MR reported in $\text{Sr}_2\text{FeMoO}_6$ (SFMO)⁸ where the MR was shown to peak at a magnetic field higher than the magnetic coercivity of the material. This, and several other qualitative deviations of the experimentally observed behavior from the case of the usual TMR systems were shown⁸⁻¹⁰ to arise from the magnetic nature of the insulating barrier layer. Essentially, the departure of the zero MR state from the coercive field was suggested to be controlled by the grain boundary material that was believed to be a hard magnetic insulator acting like a spin valve. This novel TMR mechanism has been termed as spin-valve-type magnetoresistance (SVMR)⁸ and its most essential ingredient is a magnetic insulating barrier with a coercive field higher than the coercive field of the metallic magnetic grains. It is to be noted that few known examples of SVMR relied on the grain boundary material fulfilling this criterion of being a harder magnet not by choice, but by accident. If these ideas are correct, it suggests a route to manipulate the electron tunneling process between the magnetic, metallic grains by deliberately creating an insulating, magnetic barrier whose spin orientation relative to that of the metallic grain can be controlled by the application of a suitable magnetic field. The relative orientation of the grain and the grain boundary spins will be determined by the relative strengths of the magnetic coercivities of the two parts.

In order to engineer a TMR structure with a pronounced SVMR behavior, a convenient choice would be a core-shell nanomaterial where the core is made of a soft magnetic material

with a substantial spin polarization and the shell should be a magnetic insulator with a high magnetic anisotropy and coercivity. Additionally, the spin filtering property of CoFe_2O_4 ¹¹⁻¹³ makes it a very suitable choice for the barrier layer. We find that a system composed of Fe_3O_4 (FO) core and CoFe_2O_4 (CFO) shell suits the above criteria very well. Spinel Fe_3O_4 is a well known soft magnetic material with a coercivity of few Oe¹⁴ in the bulk form and few hundred Oe for nanoparticles¹⁵ with a high degree of spin polarization.^{16,17} Fe_3O_4 polycrystalline, thin film and nanocrystal samples have been studied^{16,18,19} for its tunneling magnetoresistance property. CoFe_2O_4 also forms in spinel crystal structure and is a highly insulating magnetic material with a large coercivity, in contrast to a non-magnetic barrier.²⁰ Spin filtering property of CFO has already been reported.¹¹⁻¹³ It allows one to use non-magnetic metallic electrodes in MTJ systems, thereby widening the choice of material combinations for the study and application of tunneling magnetoresistance phenomenon. This choice also presents an added advantage due to the near perfect lattice matching between the core and the shell materials, allowing almost epitaxial growth of the shell material, CoFe_2O_4 , over the core, Fe_3O_4 . We chose a colloidal chemistry method to prepare the core-shell nanoparticles. This method is reported to produce uniform sized and high quality magnetic nanoparticles of both ordinary²¹ and core-shell²² types. Our magnetization and magnetoresistance measurements on this specifically designed core-shell TMR structure establishes the influence of the magnetic barrier on the magnetoresistance of a TMR structure unambiguously.

Fe_3O_4 nanoparticles are prepared and characterized as described in ref [16]. These Fe_3O_4 nanoparticles are used as seed particles to grow Fe_3O_4 - CoFe_2O_4 core-shell particles. To a part of the Fe_3O_4 nanoparticle solution in trioctylamine (TOA), 0.16 mmol of Co-oleate and 0.27 mmol of Fe-oleate are added which are the starting precursors for the CoFe_2O_4 shell. The relative amounts of Fe and Co precursors necessary to obtain stoichiometric CoFe_2O_4 phase is optimized in control experiments where pure CoFe_2O_4 nanoparticles were prepared and analysed using ICP-OES (Inductively Coupled Plasma - Optical Emission Spectroscopy). The reaction mixture is purged with nitrogen gas and heated to 300 °C with continuous nitrogen flow and stirring. The temperature is held at 300 °C for 15 minutes to enable the formation of CoFe_2O_4 shell on the Fe_3O_4 core. The core-shell particles are then collected after purification. The purification process involves collecting TOA in acetone after dissolving and centrifugation. The particles are then dispersed in chloroform and re-precipitated in ethanol before centrifuging to get solid powder of nanoparticles sample. A

part of this sample is pressed into a pellet by cold pressing. The pellet is then annealed under Ar gas flow at 450 °C for 2 hrs to remove organics from the surface of the particles and to ensure good inter-particle connectivity. Annealing conditions were optimized to ensure the highest connectivity between different nanocrystals, leading to a higher density and mechanical strength of the pellet, and lowering the electrical resistance between individual nanocrystals, while keeping the inter-diffusion between Fe_3O_4 and CoFe_2O_4 to a minimum. Annealing at any higher temperature resulted in a degradation of the well-defined core-shell structure as represented by drastic changes in magnetic and transport properties due to the interdiffusion between the two components.

Fe_3O_4 - CoFe_2O_4 core-shell particles are checked for phase purity using a Bruker D8 Advance x-ray diffractometer. A JEOL High Resolution Transmission Electron Microscope (HRTEM) is used for checking the particle morphology, size and size distribution, while the energy dispersive x-ray spectroscopy (EDS) is used to confirm the existence of Co in several individual particles, indicating the formation of core-shell particles and not separate particles of Fe_3O_4 and CoFe_2O_4 . Magnetic and magneto-transport properties were measured using Cryogenic and Quantum design PPMS systems. The magnetic properties are measured on both the as obtained powders and on the annealed pellets. The pellets are used for measuring magneto-transport properties.

Fe_3O_4 - CoFe_2O_4 core-shell nanoparticles form in a cubic spinel phase as confirmed from x-ray diffraction pattern (Fig. 1(a)). The HRTEM images in Figures 1(b) and 1(c) show nearly spherical particles of FO-CFO. Figure 1(d) shows the high-resolution images of individual particle with highly ordered crystal planes. The particle size distribution obtained from analysis of several TEM images is presented in Figure 1(e). This histogram is well described by the lognormal distribution function, shown by a continuous curve in the figure. This analysis establishes a diameter of 11.4 nm for FO-CFO which is distinctly larger than 10.2 nm, the diameter of Fe_3O_4 seed nanoparticles¹⁹ suggesting the growth of a few layers of CFO shell over the core FO particles.

Careful EDS spectra collected on several individual particles of FO-CFO sample using HRTEM instrument looks similar to the representative spectrum presented in Figure 1(e). Each of the examined nanoparticles contains Co in addition to Fe, providing yet another evidence for the formation of core-shell particles. A simple calculation using the mean diameters of the bare¹⁹ and core-shell nanoparticles from TEM gives a value of 9.6 atomic

percent for Co, which is close to the values of 8 to 9 atomic percent of Co estimated from the EDS analyses. However, the contrast difference between Co and Fe is not strong enough and the spatial resolution of the EDS not high enough for one to directly probe the nature of the FO-CFO interface in these core-shell nanoparticles.

From the zero-field-cooled (ZFC) and field-cooled (FC) magnetization measurements shown in Figure 2(a), we estimate the blocking temperature, T_B , of the FO-CFO particles to be ~ 220 K. It is to be noted that we do not observe any signature of a second T_B which should have existed²² if there were also independent FO and/or CFO particles along with the FO-CFO core-shell particles. It should also be noted that CoFe₂O₄ shell of ~ 0.6 nm thickness (from TEM analysis) equals to $\sim 28\%$ of the total volume of the particle of diameter ~ 11.4 nm. This and the fact that the coercivity of the Fe₃O₄ and CoFe₂O₄ differ hugely results in the observed $M(H)$ loops where only CoFe₂O₄ coercivity is prominent as shown in Figure 2(b).

Figure 2(b) presents the $M(H)$ loops, at different temperatures, of the annealed pellet of FO-CFO and the representative $M(H)$ loops of the core-shell particles, before annealing, at two temperatures are shown in the inset to Figure 2(b). Results in Figure 2(b) clearly show that $M(H)$ loops measured on the pellet and powder forms have largely different coercivity values, with the pellets of FO-CFO exhibiting a huge increase in coercivity compared to the nanoparticle powder. For example, the coercivity at 50 K, of FO-CFO increases from 800 Oe in powder form to ~ 12.3 kOe in the pellet form. This enhancement in the coercivity can be attributed to the increase in the effective crystallite size of CoFe₂O₄ in FO-CFO due to the annealing of pellet at 450 °C, since annealing of the pressed pellet helps to fuse the individual shells of CFO on neighboring nanocrystals, thereby giving rise to a continuous matrix of CFO with FO embedded in it, increasing both the coercivity of the CFO component and the mechanical strength of the pellet as a whole. Since the coercivity is clearly a pronounced function of the CFO grain size and the growth in the grain size is a thermally driven statistical process, it is clear that the moderately sintered sample has a range of grain sizes, leading to a distribution of magnetic coercivities in the sample. The $M(H)$ data in the main frame of Figure 2(b) represents a weighted average of contributions from different grain sizes in the sample.

In Figure 3, the magnetoresistance (MR), defined as $100 \times [(R(H)-R(0))/R(0)]$, of FO-CFO pellet is plotted as a function of magnetic field (H) at 50 K. A peak in the $MR(H)$

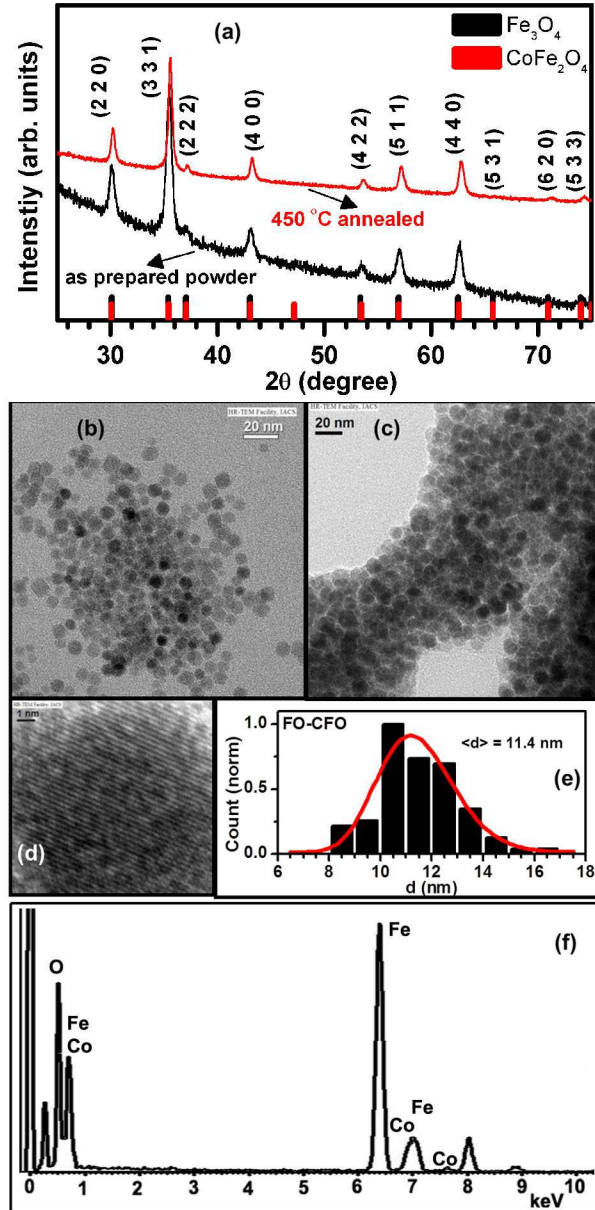


FIG. 1. (Color online) (a) The XRD pattern of the core-shell Fe_3O_4 - CoFe_2O_4 (FO-CFO) is presented. The JCPDF data (black and red bars respectively for Fe_3O_4 and CoFe_2O_4) are also presented for comparison. The TEM images of the Fe_3O_4 - CoFe_2O_4 (FO-CFO) sample are shown in panels (b) and (c), the panel (d) shows the high-resolution image of individual particle. The panel (e) shows the particle size distribution of the sample along with a lognormal curve fitting. The representative EDS data of the FO-CFO particle is given in panel (f)

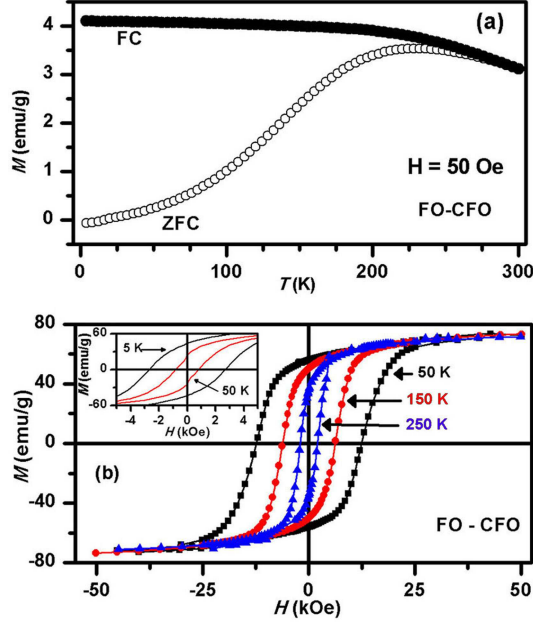


FIG. 2. (Color online) (a) The zero-field-cooled (ZFC) and field-cooled (FC) $M(T)$ data of as prepared Fe_3O_4 - CoFe_2O_4 (FO-CFO) particles, the cooling and measuring magnetic field is set as 50 Oe. The panel (b) shows the hysteresis [$M(H)$] loops of the annealed pellet of FO-CFO measured at different temperatures. The inset shows the hysteresis [$M(H)$] loops measured on as prepared FO-CFO particles for two different temperatures, 5 and 50 K.

curve represents the highest resistive state of the sample. We represent the field value at which this resistance peak occurs by H_C^{MR} , in this manuscript.

As mentioned in the introduction, one of the characteristics of conventional TMR structures is that the H_C^{MR} value of a TMR system, consisting of only one magnetic component, generally coincides with the magnetic coercivity of the metallic magnetic grains.^{3,5} This is also true for the TMR of bare Fe_3O_4 nanoparticles in absence of any CFO shell covering it.¹⁹ In presence of the CFO over layer, however, the H_C^{MR} observed for tunneling between Fe_3O_4 nanoparticles across the insulating CoFe_2O_4 barrier layer, is ~ 9 kOe at 50 K (see Fig. 3(a)) which is much higher (~ 13 times) than the H_C value of 700 Oe, of Fe_3O_4 at 50 K. We have observed similarly large discrepancy between H_C^{MR} of FO-CFO pellet compared to the H_C of Fe_3O_4 nanoparticles at other temperatures as well. This is illustrated in Figure 3(b) where H_C^{MR} of FO-CFO pellet has been plotted as a function of the H_C of Fe_3O_4 annealed pellet (extracted from Ref [16]) for three different temperatures; the dashed line represents $H_C^{MR} = H_C$ line, clearly showing more than an order of magnitude enhancement of H_C^{MR}

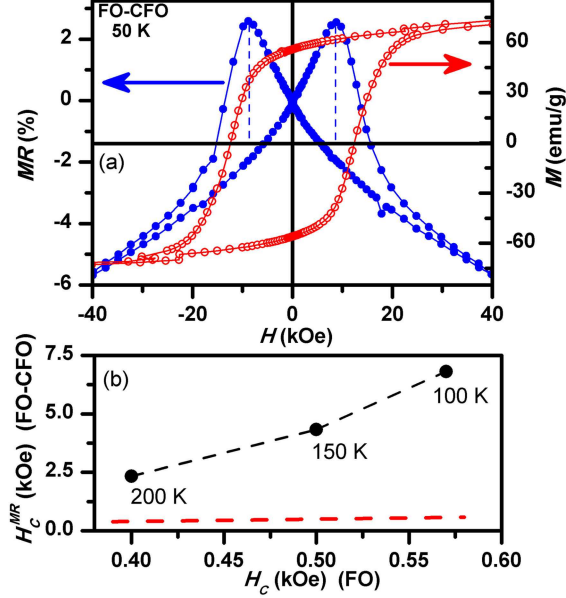


FIG. 3. (Color online) Representative plots, measured at 50 K, of magnetoresistance, (MR) and magnetization, M as a function of applied magnetic field, (H) of FO-CFO are shown in the panel (a). In panel (b), H_C^{MR} values of FO-CFO sample are plotted as a function of H_C of Fe_3O_4 , for different temperatures. Since the scales for the two axes in Fig. 3(b) differ by more than an order of magnitude, we provide a dashed line representing $H_C^{MR} = H_C$ of FO as a guide. This line shows the expected behavior of H_C^{MR} , if the tunnel barrier would be non-magnetic, thereby emphasizing the more than an order of magnitude enhancement of H_C^{MR} on making the barrier magnetic.

compared to the coercive field of Fe_3O_4 grains over the entire temperature range. Having established the irrelevance of the magnetic coercivity of the Fe_3O_4 nanoparticles in determining the H_C^{MR} of the tunneling magnetoresistance between Fe_3O_4 nanoparticles separated by highly insulating $CoFe_2O_4$, we now show that H_C^{MR} of the system is, in fact, controlled by the magnetic coercivity of the barrier layer, as proposed for the spin-valve type magnetoresistance in the case of SFMO,^{8,10} in contrast to the usual TMR behavior. This is illustrated in Figure 4, by plotting H_C^{MR} and H_C of the sample as a function of the temperature. It is to be noted that the coercive fields of Fe_3O_4 and $CoFe_2O_4$ are so vastly different that the coercive field of the sample, seen in Figure 2, is essentially controlled entirely by the $CoFe_2O_4$ component of the sample. It is clear from Figure 4 that H_C^{MR} is similar to H_C at all temperatures, evidencing the control of the highest resistive peak in the MR of the sample by the coercive field of the barrier layer, and not by the coercive field of the Fe_3O_4 grains,

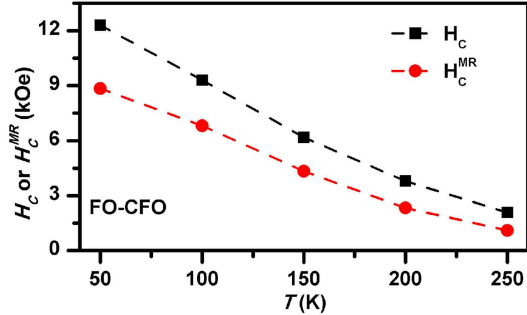


FIG. 4. (Color online) (a) A comparison of magnetic coercivity, H_C and the magnetoresistance coercivity, H_C^{MR} of FO-CFO for different measurement temperatures is presented.

thereby establishing itself as an ideal example of a specifically engineered SVMR system. Here we note that the systematic (28-47%) reduction of the H_C^{MR} compared to H_C is easy to understand. As already mentioned while discussing $M(H)$ plots of the sample in Figure 2, the sample is expected to be magnetically inhomogeneous to some extent, depending on the growth of the effective grain size of CoFe_2O_4 at various locations in the sample on annealing. The tunneling conductivity will be dominated by the thinnest CFO barrier layer separating the Fe_3O_4 grains and the coercivity of such thin parts of the CFO layer is indeed expected to be lower than the coercivity of the entire sample, averaged over all layer sizes. Thus, the magnetoresistance of the sample will reflect a somewhat lower coercivity than the average value, as indeed shown in Figure 4. It is instructive at this stage to compare the behavior of MR in a system with Fe_3O_4 nanoparticles alone¹⁹ and in the present system using Fe_3O_4 - CoFe_2O_4 core-shell nanostructured material. It has been shown¹⁹ that MR in the Fe_3O_4 system can be well understood in terms of the expected behavior of a traditional TMR material. It is important to note here that the MR value of the present FO-CFO sample remains almost same as that for the Fe_3O_4 sample at comparable magnetic fields and identical temperatures. On the other hand, clearly we are able to influence the peak position of $MR(H)$ in the core-shell system to make it larger than in the Fe_3O_4 system by more than a factor of ten. This clearly establishes that an artificial SVMR system can be engineered with controllable magnetic properties of the tunnel barrier. In addition, we would also like to point out another difference in the $MR(H)$ curves of Fe_3O_4 and FO-CFO samples. From Figure 3(a), it can be observed that the drop in resistance (or in MR), after the peak, is sharp in the case of FO-CFO compared to the behavior of $MR(H)$ for Fe_3O_4 alone. This sharper response in MR in the case of FO-CFO system is consistent with the idea that the

tunneling current in this system is controlled by the spin-valve type mechanism and can be understood in the following terms. For $H < H_C^{MR}$ even though the magnetic field is sufficient to saturate the FO core moment¹⁹, the tunneling current is blocked until the tunnel barrier magnetically aligns with the FO core and for $H > H_C^{MR}$ the tunneling current is allowed suddenly, leading to a sharp fall in resistance (or in MR). It should also be noted that the MR results observed in FO-CFO are distinctly different from the MR results on Co doped Fe_3O_4 ²³ where no sharp fall in resistance is observed and further a clear reduction in $MR\%$ compared to undoped Fe_3O_4 due to loss of spin-polarization with Co doping is also reported.

In conclusion, magnetoresistance properties of a tunneling magnetoresistance system with a magnetic tunnel barrier are studied by using a specifically engineered core-shell nanoparticle structure, Fe_3O_4 - $CoFe_2O_4$, as a model system. It is observed that the highest resistive state of such a system is essentially controlled by the magnetic coercivity of the tunnel barrier in contrast to the standard TMR behavior and defining a spin-valve type MR system. In addition, the magnetoresistance value of the core-shell nanoparticle system is comparable to the bare Fe_3O_4 nanoparticle system indicating that the spin polarization for Fe_3O_4 core is not diminished in the present case unlike in Co doped Fe_3O_4 samples. Thus, our results provide an alternate route to manipulate the magnetoresistance behavior of a TMR system by using spin-valve like action of the hard magnetic barrier layer without any quantitative degradation of the MR.

Authors thank Department of Science and Technology for supporting this research. PAK thanks the Swedish Research Council (VR) and the Göran Gustafsson Foundation, Sweden for funding. SC acknowledge support by the Japan Society for the Promotion of Science (JSPS) through the “Funding Program for World-Leading Innovative R&D on Science and Technology (FIRST Program)”.

REFERENCES

- ¹M. Julliere, Phys. Lett. A **54**, 225–226 (1975).
- ²J. S. Moodera, L. R. Kinder, T. M. Wong, and R. Meservey, Phys. Rev. Lett. **74**, 3273–3276 (1995).
- ³J. M. D. Coey, A. E. Berkowitz, L. Balcells, F. F. Putris, and A. Barry, Phys. Rev. Lett.

- 80**, 3815–3818 (1998).
- ⁴J. M. D. Coey, A. E. Berkowitz, L. Balcells, F. F. Putris, and F. T. Parker, *Appl. Phys. Lett.* **72**, 734–736 (1998).
- ⁵X. W. Li, A. Gupta, G. Xiao, and G. Q. Gong, *Appl. Phys. Lett.* **71**, 1124–1126 (1997).
- ⁶H. Y. Hwang, S. W. Cheong, N. P. Ong, and B. Batlogg, *Phys. Rev. Lett.* **77**, 2041–2044 (1996).
- ⁷P. Anil Kumar and D. D. Sarma, *Appl. Phys. Lett.* **100**, 262407 (2012).
- ⁸D. D. Sarma, S. Ray, K. Tanaka, M. Kobayashi, A. Fujimori, P. Sanyal, H. R. Krishnamurthy, and C. Dasgupta, *Phys. Rev. Lett.* **98**, 157205 (2007).
- ⁹S. Jana, S. Middey, and S. Ray, *J. Phys.: Condens. Matter.* **22**, 346004 (2010).
- ¹⁰S. Ray, S. Middey, S. Jana, A. Banerjee, P. Sanyal, R. Rawat, L. Gregoratti, and D. D. Sarma, *Europhys. Lett.* **94**, 47007 (2011).
- ¹¹A. V. Ramos, M.-J. Guittet, J.-B. Moussy, R. Mattana, C. Deranlot, F. Petroff, and C. Gatel, *Appl. Phys. Lett.* **91**, 122107 (2007).
- ¹²S. Matzen, J.-B. Moussy, R. Mattana, K. Bouzehouane, C. Deranlot, and F. Petroff, *Appl. Phys. Lett.* **101**, 042409 (2012).
- ¹³A. V. Ramos, T. S. Santos, G. X. Miao, M.-J. Guittet, J.-B. Moussy, and J. S. Moodera, *Phys. Rev. B* **78**, 180402 (2008).
- ¹⁴O. Ozdemir, *Geophys. J. Int.* **141**, 351–356 (2000).
- ¹⁵D. Caruntu, G. Caruntu, and C. J. O’Connor, *J. Phys. D* **40**, 5801–5809 (2007).
- ¹⁶H. Liu, E. Y. Jiang, H. L. Bai, R. K. Zheng, H. L. Wei, and X. X. Zhang, *Appl. Phys. Lett.* **83**, 3531–3533 (2003).
- ¹⁷M. Fonin, Y. Dedkov, C. Konig, G. Guntherodt, U. Rudiger, J. Mayer, D. Vyalikh, and S. Molodtsov, *Adv. in Solid State Phys.* **43**, 487–503 (2003).
- ¹⁸X. W. Li, A. Gupta, G. Xiao, and G. Q. Gong, *J. Appl. Phys.* **83**, 7049–7051 (1998).
- ¹⁹P. Anil Kumar, S. Ray, S. Chakraverty, and D. D. Sarma, *J. Exp. Nanosci.* **0**, 1–7 (2012).
- ²⁰C. N. Chinnasamy, B. Jeyadevan, K. Shinoda, K. Tohji, D. J. Djayaprawira, M. Takahashi, R. J. Joseyphus, and A. Narayanasamy, *Appl. Phys. Lett.* **83**, 2862–2864 (2003).
- ²¹J. Park, K. J. An, Y. S. Hwang, J. G. Park, H. J. Noh, J. Y. Kim, J. H. Park, N. M. Hwang, and T. Hyeon, *Nature Mater.* **3**, 891–895 (2004).
- ²²O. Masala, D. Hoffman, N. Sundaram, K. Page, T. Proffen, G. Lawes, and R. Seshadri, *Solid. State. Sci.* **8**, 1015–1022 (2006).

²³D. Tripathy, A. O. Adeyeye, C. B. Boothroyd, and S. N. Piramanayagam, *J. Appl. Phys.* **101**, 013904 (2007).